RSC Pharmaceutics

ROYAL SOCIETY OF CHEMISTRY

PAPER

View Article Online
View Journal | View Issue

Open Access Article. Published on 01 August 2024. Downloaded on 10/16/2025 6:11:21 PM.
This article is licensed under a Creative Commons Attribution-NonCommercial 3.0 Unported Licence.

Check for updates

Cite this: *RSC Pharm.*, 2024, **1**, 797

Functionalized SBA-15: engineering, detailed study on release and kinetics of alendronate as well as its anti-tumour properties towards osteosarcoma

Anjali Patel * and Shivangi Mehta

Received 16th March 2024,
Accepted 19th July 2024

DOI: 10.1039/d4pm00078a

rsc.li/RSCPharma

The present work deals with designing a biocompatible controlled drug delivery system (DDS) based on 12-tungstophosphoric acid (TPA)-functionalized SBA-15 for anti-osteoporotic drug alendronate sodium (ALD) and its characterization using different physicochemical techniques such as TGA, FT-IR spectroscopy, XRD, N_2 adsorption measurements, HRTEM, and SEM. The designed DDS, ALD/TPA/SBA-15, was assessed for its drug delivery potential by carrying out *in vitro* drug release in simulated body fluid (pH 7.4, 37 °C) under stirring conditions as well as for the dissolution study. Release kinetics and mechanisms using zero order, first order, and Higuchi model were also carried out. Further, the release profile of the designed DDS was compared with the available marketed formulation (Osteofos), and ALD/TPA/SBA-15 shows a more controlled release. To explore the direct anti-tumour potency of ALD on osteosarcoma cells, an MTT assay was carried out at different concentrations, and the results show concentration-dependent inhibition of osteosarcoma cell proliferation.

Introduction

The microarchitectural deterioration of bony tissue and low bone density leads to a skeletal disorder known as osteoporosis.[1] As there are no symptoms before fracture occurs, this medical condition is a "silent epidemic". It is primarily an underrated and undertreated condition, and nearly 200 million people are suffering from this worldwide. World Health Organization (WHO) defines osteoporosis based on the *T*-score obtained from bone mineral density measurement (BMD), which says that if a *T*-score is more than 2.5 BMD in young adults, then osteoporosis is diagnosed.[2,3] This condition emerges due to alteration in the bone remodelling process, which comprises removing old bone (osteoclast) and forming new bone (osteoblast).[4]

Osteoporosis can be treated using anti-osteoporotic drugs. Anti-osteoporotic drugs maintain bone remodelling, reduce bone resorption and enhance bone formation. In the 1960s, the biological effect of bisphosphonates was studied for the first time, and it evolved into medicine for osteoporosis. Bisphosphonates are pyrophosphate analogues, containing the P–C–P bond covalently with the attached two side chains, A and B.[5] Nitrogen-containing bisphosphonates are currently used as the first-line medicine for the treatment of osteoporosis. Amongst bisphosphonates, ALD has been widely used for healing postmenopausal osteoporosis, Paget disease, and metastatic bone disease. According to biopharmaceutical classification (BCS), alendronate falls in the class III category (high solubility and low permeability due to its polar hydrophilic nature), which indicates that its bioavailability is very low and oral absorption is limited. The lower bioavailability causes higher dosages of drug that leads to side effect, including the irritation of the upper gastrointestinal tract and necrosis of the jaws. The oral administration of ALD leads to severe musculoskeletal pain and cardiovascular risks. Intravenous delivery leads to nephrotoxicity due to complex formation with calcium.[6]

To address the above-mentioned limitations, controlled drug delivery systems have been developed, which can monitor the amount of drug released and possess some advantages such as decreasing the toxic effects and reducing the side effects. The system's effectiveness depends on the carrier compatibility, which can load a higher amount of drug and fail to release it prematurely. In this regard, several drug delivery systems, including polymeric nanoparticles, lipid particles, nanoparticles, microsphere, mesoporous carbon, MOF, calcium phosphate, hydrogel, scaffolds, and mesoporous silica, have been investigated as carriers for ALD, which are mentioned therein.[5]

Mesoporous silica-based materials are excellent carriers for drug delivery applications. Controlled release and high drug encapsulation can be achieved as this material has a larger surface area and pore volume.[7] Moreover, modifications can be made to the silica material's surface to slow the release rate. A literature review indicates that only four reports are available using mesoporous silica material as a delivery system

Department of Chemistry, Faculty of Science, The Maharaja Sayajirao University of Baroda, Vadodara, 390002, India. E-mail: anjali.patel-chem@msubaroda.ac.in

© 2024 The Author(s). Published by the Royal Society of Chemistry

Open Access Article. Published on 01 August 2024. Downloaded on 10/16/2025 6:11:21 PM.
This article is licensed under a Creative Commons Attribution-NonCommercial 3.0 Unported Licence.

for the controlled release of ALD. In 2006, Balas *et al.* employed SBA-15 and MCM-41 as a delivery system for ALD.[8] With that, functionalisation was done by the aminopropyl group.[9] Employing this, there is an increase in drug intake capacity from 1% to 40%. Also, the adsorption capacity increases three times after functionalisation. In 2010, Colilla *et al.* employed another modification on SBA-15 by the phosphorus group.[10] It shows that complete release can be achieved in 10 days, and *in vitro* bioactivity assays show that an apatite-like layer was able to form in the phosphorus-containing SBA-15 samples, which accelerates the bone repair process. In 2016, Tantaru *et al.* employed MCM-41 and MCM-48 as drug delivery carriers for ALD without any functionalising agent.[11] It shows that MCM-41 have burst effect with a release of 45.55% in 2 hours, and MCM-48 shows a slower release of 82.49% in 24 hours. In 2018, Ha *et al.* explored MCM-41 and phosphorylcholine-functionalized MCM-41 as drug delivery carriers for ALD. They showed 60% drug release in 2 and 4 days, respectively.[12]

It is noted that SBA-15 has been functionalized using aminopropyl and phosphorus groups; thus, it would be of interest to use an inorganic moiety for the functionalization of SBA-15. Heteropolyacids are excellent candidates with known medical applications.[13] The critical component of heteropolyacids is the presence of non-bonded oxygen in their structure, which may bind to different functional groups. Negatively charged metal–oxygen clusters, such as W(VI), Mo(VI), and V(V), are known as HPAs. The most widely accessible Keggin type heteropolyanion has the general formula $[Xn^{n+}M_{12}O_{40}]^{(8-n)-}$, in which M is an addenda atom (W^{6+}, Mo^{6+}, V^{5+}, *etc.*) and Xn^{n+} is a central heteroatom (Si^{4+}, P^{5+}, *etc.*). According to a literature review, 12-tungstophosphoric acid (TPA) is often utilized in medicinal chemistry.[14,15]

The present study aims to design a drug delivery system for the controlled release of ALD. It describes the synthesis of TPA/SBA-15 and its characterization using SEM, TGA, FT-IR, XRD, N_2 adsorption measurements, and HRTEM analysis. *In vitro* release studies of unfunctionalized (SBA-15) and functionalized (TPA/SBA-15) were carried out in simulated body fluid (SBF-7.4) at 37 °C under stirring conditions to study the role of TPA as a functionalizing agent for the release of ALD. Further, the release study was carried out under the same conditions for the marketed formulation of ALD, *i.e.*, Osteofos, and it was compared with release studies of the synthesized material. Moreover, release studies were also carried out in the dissolution apparatus for synthesized materials. Different models, such as zero order, first order, and Higuchi model, were explored to study the kinetics and mechanism.

In addition to ALD's therapeutic activity, preclinical and clinical evidence shows that N-BP has anti-cancer potential that may be attributed to its effect on other cells rather than osteoclasts.[16] Moreover, there were reports on the inherent antitumor activity of N-BP, including tumour cell apoptosis and inhibition of tumour cell growth.[17] Hence, it was decided to assess the cytotoxic effect of the designed system using an MTT assay using an MG-63 cell line.

Experimental

Materials

Alendronate Sodium Trihydrate (ALD) was purchased from TCI. Tetraethyl orthosilicate (TEOS), 12-tungstophosphoric acid (TPA), Pluronic-123 and hydrochloric acid were purchased from Merck. All the chemicals were of A.R. grade and used without any further purification. Osteofos (each tablet containing 35 mg of Alendronic acid), a marketed formulation of Alendronate Sodium Trihydrate, was obtained from a pharmaceutical store.

Synthesis of SBA-15

The synthesis of SBA-15 was carried out using the reported procedure.[18] 4 g of Pluronic 123 surfactant was dissolved in 30 mL water with 120 mL and 2 M HCl at 35 °C. After the completely dissolved surfactant, 4.3 g of TEOS, a silica source, was added with stirring for 20 h. The resultant white mixture was aged at 80 °C for 48 h. The final product was washed with distilled water, dried at 100 °C, followed by calcination at 500 °C for 6 h, and the obtained material was designated as SBA-15.

Functionalization of SBA-15 by 12-tungstophosphoric acid (TPA)

A wet impregnation method was used for the functionalization of SBA-15. 1 g of SBA-15 was functionalized using 30% (0.3/30 g mL^{-1} of distilled water) of TPA and then dried at 100 °C for 10 h. The obtained material was designated as TPA/SBA-15.[18]

Loading of alendronate (ALD) into SBA-15 and TPA/SBA-15

A 1.0 mg mL^{-1} solution of ALD was obtained by dissolving 10 mg of the drug in 10 mL of water to load ALD. To make a 1 : 1 (Drug : Carrier) ratio, 10.0 mg of SBA-15 was suspended in 10 mL of the 1.0 mg mL^{-1} drug solution. The solution was then stirred for 24 hours to complete the loading of the drug into the pores of SBA-15. After 24 h, the particles were isolated using centrifugation. The particles were washed thoroughly with acetone to remove excess of the drug. Then, the drug-loaded particles were air-dried and stored. The obtained material was termed as ALD/SBA-15. The same method was used to load ALD on TPA/SBA-15; the resulting material was termed as ALD/TPA/SBA-15.

The amount of drug encapsulated was calculated using the absorbance of the loading media.[19] A calibration plot (Fig. 1) for ALD at 568 nm was used to measure the free drug concentration in the supernatant. Using the following equation, the % encapsulation efficiency of the drug was calculated as

$$\%\text{Encapsulation Efficiency} = \frac{E_c - E_s}{E_c} \times 100,$$

where E_c denotes the initial concentration of ALD taken, while E_s denotes the concentration of the drug in the supernatant solution.

The calibration curve was plotted as follows: stock solution of ALD was prepared with a concentration of 0.2 mg mL^{-1}. Since ALD is UV inactive, it was derivatized with ninhydrin according to the reported procedure.[20,21] Typically, 0.2% nin-

 © 2024 The Author(s). Published by the Royal Society of Chemistry

Open Access Article. Published on 01 August 2024. Downloaded on 10/16/2025 6:11:21 PM.
This article is licensed under a Creative Commons Attribution-NonCommercial 3.0 Unported Licence.

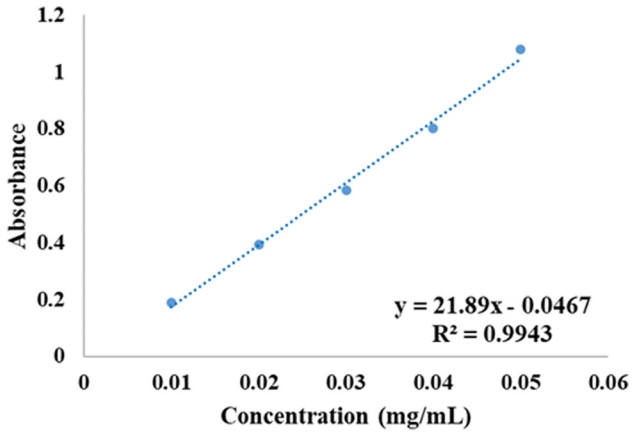

Fig. 1 Calibration curve of ALD.

hydrin solution was prepared in methanol and 0.05 mol L^{-1} sodium bicarbonate aqueous solution. Different aliquots of standard stock solution equivalent to 0.01–0.06 mg mL^{-1} were transferred into a series of 10 mL Nessler's tubes, then 2.5 mL ninhydrin solution and 0.5 mL of sodium bicarbonate solution were added. This was followed by heating the mixture in a water bath at 100 °C for 20 min. The mixture was then cooled down and distilled water was added to make up a volume of up to 10 mL and analyzed using a PerkinElmer Lambda 35 UV-Vis Spectrophotometer instrument.

Characterization

TGA analysis was done on a Mettler Toledo Star SW 7.01 from 30 °C to 500 °C at a heating rate of 10 °C min^{-1} in a nitrogen atmosphere. Using a KBr pellet, the FT-IR spectra of materials were recorded. The XRD pattern was obtained using a PHILIPS PW-1830. The conditions used were: Cu K radiation (1.5417 Å), scanning angle from 0° to 10°. Desorption isotherm was recorded on a Micromeritics ASAP 2010 surface area analyzer at liquid nitrogen temperature. High-resolution transmission electron microscopy (HRTEM) was carried out on a JEOL TEM instrument (model-JEM 2100) with a 200 kV acceleration voltage. The samples were dispersed ultrasonically and sprayed on a grid before drying in air overnight. SEM analysis was performed on a JSM-7600F FEG-SEM analyzer. Our group has already published detailed characterizations related to SBA-15 and TPA/SBA-15; however, some are included for comparison and the reader's convenience.[18]

Drug release study

The release curve was established by plotting the amount of drug released with the progression of time. In SBF (pH 7.4), the drug release experiments were carried out. 5 mg of ALD/SBA-15 was suspended in a 10 mL release medium and kept at 37 °C with constant stirring. Aliquots from the release media were taken at different times to measure the ALD release. An identical quantity of fresh-release medium was added to each sample that was taken out. The same procedure was followed for ALD/TPA/SBA-15 as well as for the marketed formulation, Osteofos (with equivalent active amount of drug).

Since ALD is UV inactive, aliquots previously taken were derivatized with ninhydrin according to the reported method.[20,21] 0.5 mL of ALD solution was mixed with 2.5 mL of 0.2% ninhydrin solution and 0.5 mL of 0.05 mol L^{-1} sodium bicarbonate solution. This was followed by heating the mixture in a water bath at 100 °C for 20 min. The mixture was then cooled down, and distilled water was added to make a volume of up to 10 mL and analyzed in a UV-Vis spectrophotometer.

Dissolution study

The experiment was carried out in SBF (pH 7.4). 5 mg of ALD/SBA-15 was suspended in a release medium and kept at 37 °C with constant stirring with the help of a paddle. Aliquots from the release media were obtained at various time intervals to determine ALD release. Each withdrawn sample was replenished with the same amount of fresh-release medium. The same procedure was used for ALD/TPA/SBA-15 and for the marketed formulation using an equivalent active amount of the drug. The amount of drug release was calculated using the method discussed in section "Drug release study".

In vitro study-MTT assay

The cytotoxicity assay was performed on an MG-63 cell line (Osteosarcoma) procured from the National Centre of Cell Science (NCCS), Pune, India. The cells were maintained in a CO_2 incubator with 5% CO_2 and 95% humidity atmosphere supplemented with MEM (E) with NEAA + Na Pyruvate, 10% FBS, and penicillin and streptomycin at 1× final concentration from a 100× stock. Once the cells attained confluent growth, the cells were trypsinized using Trypsin-EDTA and the cells (10^5) were seeded into sterile 96-well plates for assays. 100 μL of treated cells were incubated with 50 μL of MTT at 37 °C for 3 hours. After incubation, 200 μL of PBS was added to all the samples and aspirated carefully to remove excess MTT. 200 μL of acid-propanol was added and left overnight in the dark for solubilization. The absorbance was read at 650 nm in a microtiter plate reader (Bio RAD U.S.A.). The percentage of cell viability was determined by comparing it with the control. The optical density of the control cells was fixed to be 100% viable, and the per cent viability of the cells in the other treatment groups was calculated using the formula

$$\%\text{Viability} = \frac{\text{OD}_{\text{Control}} - \text{OD}_{\text{Sample}}}{\text{OD}_{\text{Control}}} \times 100.$$

Results and discussion

Characterization

TGA analysis of SBA-15 (Fig. 2) occurs in two stages, with the first loss of 8.4% may be due to the loss of adsorbed water molecules. The final weight loss of 3.2% above 450 °C may be due to the condensation of silanol groups to form siloxane bonds. TPA-SBA-15 shows a first weight loss of 16.7% due to

Open Access Article. Published on 01 August 2024. Downloaded on 10/16/2025 6:11:21 PM.
This article is licensed under a Creative Commons Attribution-NonCommercial 3.0 Unported Licence.

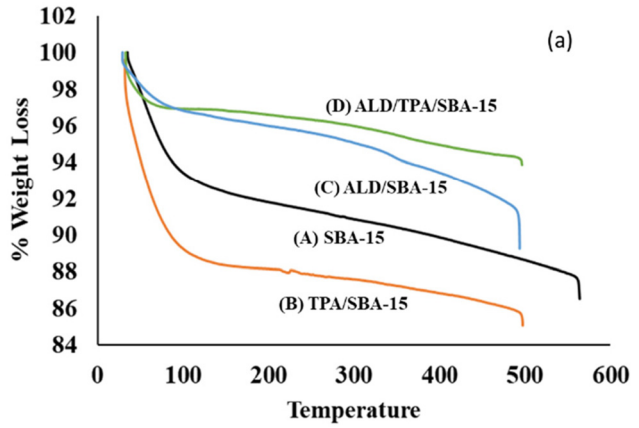

Fig. 2 (a) TGA curves of (A) SBA-15, (B) TPA-SBA-15, (C) ALD/SBA-15, (D) ALD/TPA/SBA-15.

the loss of adsorbed water. The second weight loss of 4.5% between 150 and 250 °C corresponds to the loss of water of crystallization of the Keggin ion. At higher temperatures, there is no further weight loss, which shows the stability of TPA-SBA-15.[15] Pure drug ALD shows weight loss in three stages (Fig. 3). The first weight loss of 1.4% is due to adsorbed water, and the second weight loss of 18.8% is due to ammonia release in the degradation of the drug. A final weight loss of 25.0% occurs due to the thermal degradation of the drug.[22] There is a formation of $NaH_3P_2O_7$ due to complete pyrolysis, which leads to final weight loss.[23] ALD/SBA-15 shows weight loss in three stages. The first weight loss of 3.0% is due to the loss of adsorbed water. The second weight loss of 2.4% is due to the mass loss of ammonia released during the degradation of the drug. A final weight loss of 2.4% leads to the thermal degradation of the drug. ALD/TPA/SBA-15 also shows weight loss in three stages. The first weight loss of 1.0% is due to the loss of adsorbed water. The second weight loss of 2.4% is due to the mass loss of ammonia released during the degradation of the drug. The final weight loss of 2.2% leads to the thermal degradation of the drug (Table 1).

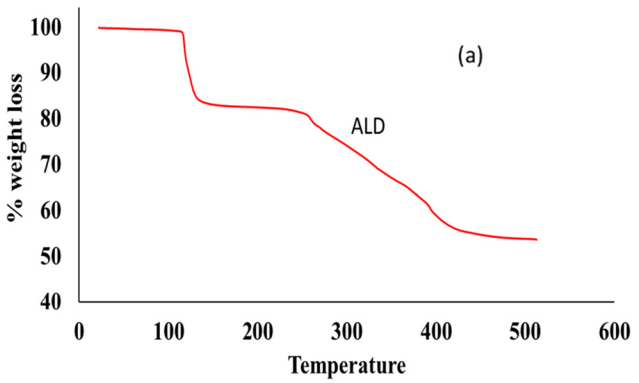

Fig. 3 (a) TGA curve of drug ALD.

Table 1 TGA degradation studies of the drug and carrier

Materials	1st Weight loss	2nd Weight loss	3rd Weight loss
SBA-15	8.4%	3.2%	—
TPA/SBA-15	16.7%	4.5%	—
ALD	1.4%	18.8%	25%
ALD/SBA-15	3%	2.4%	2.4%
ALD/TPA/SBA-15	1%	2.4%	2.2%

The FT-IR bands with frequency and FT-IR spectra (SBA-15, TPA, TPA SBA-15, ALD, ALD/SBA-15, ALD/TPA/SBA-15) are presented in Table 2 and Fig. 4, respectively. The fingerprint bands indicate that the primary structure of TPA remains intact even after impregnation. The corresponding bands with frequency of ALD were present in the FT-IR spectra of ALD/SBA-15 and ALD/TPA/SBA-15. This demonstrates that ALD was successfully loaded.

Fig. 5 shows the XRD patterns of SBA-15 and TPA/SBA-15. Three well resolved peaks at 0.89°, 1.50° and 1.72°, which are indexed to the (100), (110) and (200) reflections of the ordered hexagonal mesophase, as shown by the XRD patterns of SBA-15. In TPA/SBA-15, the intensity of peaks corresponding to the (110) and (200) planes of SBA-15 decreases. Further, the comparison of the XRD patterns of SBA-15 and TPA/SBA-15 demonstrates that the mesoporous structure of SBA-15 remains intact even after functionalization.[24]

According to IUPAC classification, all the isotherms are of type IV with H1 hysteresis loop, a characteristic of mesoporous materials.[25] A significant decrease in surface area, pore volume, and pore diameter was obtained from BET (Fig. 6).

Table 2 FT-IR bands of the synthesized materials

Compounds	Major peaks (cm^{-1})	Corresponding bands
SBA-15	1100	Asymmetric stretching of Si–O–Si
	1165	Asymmetric stretching of Si–O–Si
	801	Symmetric stretching of Si–O–Si
	463	Bending vibration of Si–O–Si
	968	Symmetric stretching vibration of Si–OH
	3448	Si–OH group
TPA	1088	P–O symmetric stretching
	987	W–O–W bending
	800	W–O
	3421	OH group (adsorbed water)
TPA/SBA-15	981	W═O stretching
	897	W–O–W stretching
	1100	Asymmetric stretching of Si–O–Si
	3460	OH group (adsorbed water)
ALD	917	P–O stretching
	1018	P–C stretching
	1048	P═O stretching
	1542	Phosphate group
	3483	N–H stretching
ALD/SBA-15	3456	N–H stretching
	467	Bending vibration of Si–O–Si
	1086	P═O stretching
ALD/TPA/SBA-15	805	W–O
	3462	N–H stretching
	461	Bending vibration of Si–O–Si

 © 2024 The Author(s). Published by the Royal Society of Chemistry

Open Access Article. Published on 01 August 2024. Downloaded on 10/16/2025 6:11:21 PM.
This article is licensed under a Creative Commons Attribution-NonCommercial 3.0 Unported Licence.

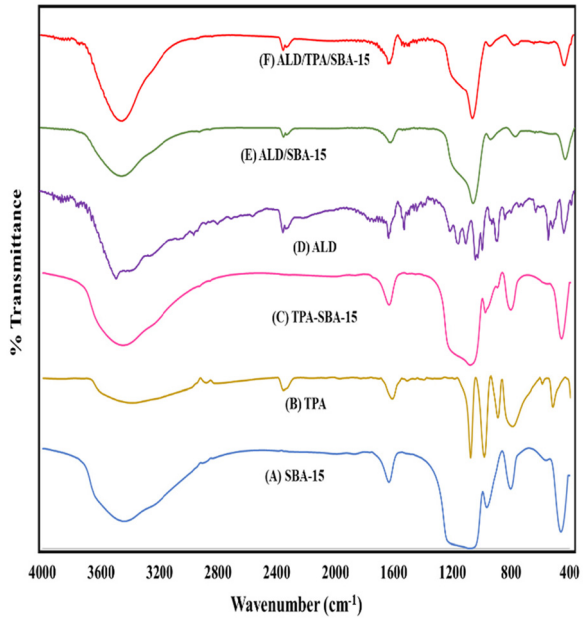

Fig. 4 FTIR spectra of (A) SBA-15, (B) TPA, (C), TPA/SBA-15, (D) ALD, (E) ALD/SBA-15, (F) ALD/TPA/SBA-15.

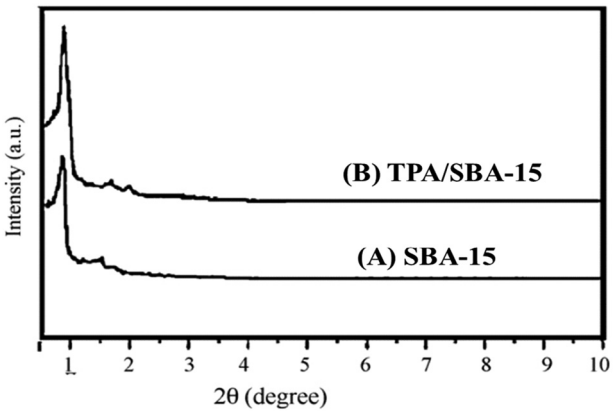

Fig. 5 Small angle XRD of (A) SBA-15 and (B) TPA/SBA-15.

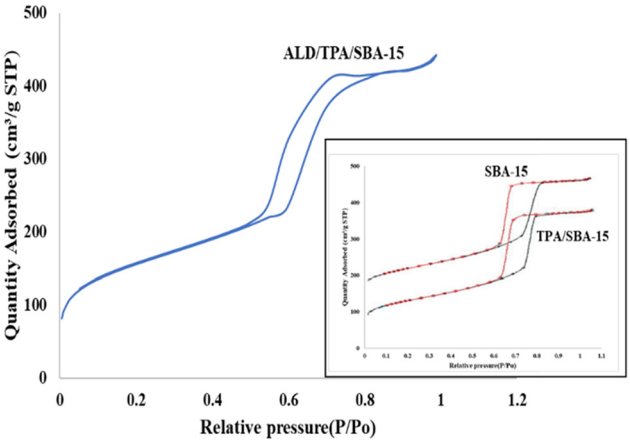

Fig. 6 Nitrogen (N_2) adsorption–desorption isotherm of ALD/TPA/SBA-15.

The reduction in the surface area for TPA/SBA-15 compared to SBA-15 indicates the effective filling of pores by TPA. Also, TPA does not affect the structure, and it remains intact after functionalization. Further, it is observed that there is an evident decrease in both the surface area and pore volume in the case of ALD/TPA/SBA-15 compared to TPA/SBA-15 and SBA-15, which shows the successful encapsulation of ALD into the pores (Table 3).

The TEM images of SBA-15 show uniform pore size and morphology of a 2D hexagonal array of channels (Fig. 7). No agglomeration shows that ALD has been homogeneously distributed. The uniform structure of SBA-15 was well maintained throughout the structure even after functionalization, which reveals that TPA species were well dispersed. The TEM images

Table 3 The textural features of SBA-15, TPA/SBA-15, and ALD/TPA/SBA-15

Material	Specific surface area ($m^2\ g^{-1}$)	Pore volume ($cm^3\ g^{-1}$)	Pore diameter (nm)
SBA-15	834	1.26	6.8
TPA/SBA-15	714	1.11	6.2
ALD/TPA/SBA-15	566	0.69	4.8

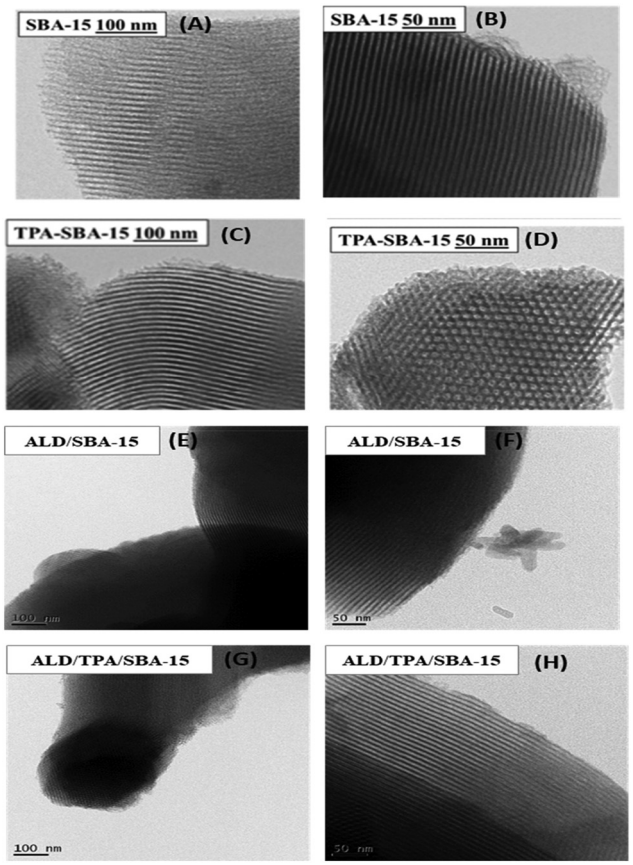

Fig. 7 HRTEM micrograph of (A and B) SBA-15, (C and D) TPA-SBA-15, (E and F) ALD/SBA-15, (G and H) ALD/TPA/SBA-15.

Open Access Article. Published on 01 August 2024. Downloaded on 10/16/2025 6:11:21 PM.
This article is licensed under a Creative Commons Attribution-NonCommercial 3.0 Unported Licence.

of ALD/TPA/SBA-15 show similar morphology and no agglomeration, indicating the good dispersion of ALD into TPA/SBA-15.

The SEM images (Fig. 8) show the external morphology of the carrier. No agglomeration in [Fig. 8(B)] shows that the loading of ALD has been successful.

In vitro release study

From UV-visible analysis, the entrapment efficiency of ALD in SBA 15 was 93%, while for TPA/SBA-15, it was 91%. This decrease in entrapment efficiency may be due to the blocking of the pores of SBA-15 by TPA during functionalization.

To study the role of TPA, the release profile of ALD from ALD/SBA-15 and ALD/TPA/SBA-15 was carried out in SBF at pH 7.4 and 37 °C under stirring conditions. Relatively slower release is obtained for ALD/TPA/SBA-15 compared to ALD/SBA-15. At 1.5 h, 29% of the drug is released for ALD/SBA-15, while in the case of ALD/TPA/SBA-15, 24% of the drug is released. It reached 95% for ALD/SBA-15 and 64% for ALD/TPA/SBA-15 in 4.5 h. This shows a slower release in the case of ALD/TPA/SBA-15 (Fig. 9). The reason could be the interaction of drug molecules with available terminal oxygen of TPA. As a result, functionalization with TPA reduces the release rate and results in a more controlled release of ALD.

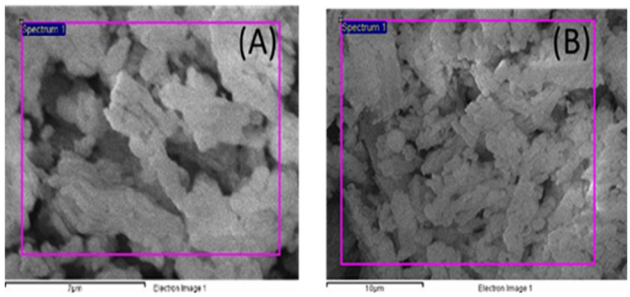

Fig. 8 SEM images of (A) TPA/SBA-15 (B) ALD/TPA/SBA-15.

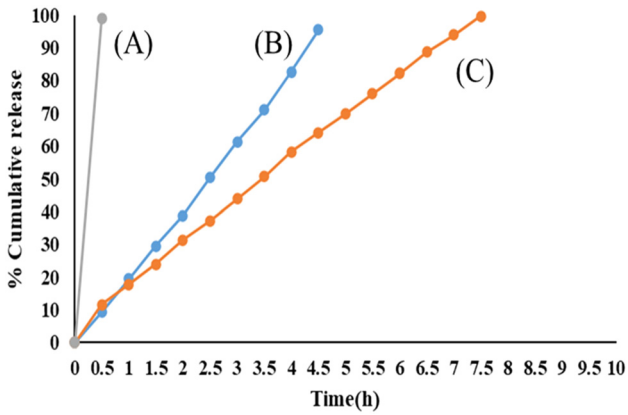

Fig. 9 *In vitro* release profiles of (A) a marketed formulation, (B) ALD/SBA-15, (C) ALD/TPA/SBA-15, and at pH 7.4.

A controlled release profile of ALD is obtained for ALD/TPA/SBA-15 amongst all the designed DDSs, and when compared with that of the marketed formulation, a better release profile is obtained. The FT-IR spectrum of ALD/TPA/SBA-15 was recorded after the release study (Fig. 10). The spectra are similar to TPA/SBA-15, indicating that TPA acts as a functionalizing agent and its structure remains intact after drug release.

Comparison with the marketed drug

Table 4 compares the release study of ALD/TPA/SBA-15 and the marketed available formulation of ALD (Osteofos). It can be observed from the table that when compared to the marketed formulation, ALD/TPA/SBA-15 shows a more delayed and controlled release profile. Dissolution studies further supported this.

Dissolution studies

Dissolution studies are done to optimize the drug release from formulations; they measure the drug release rate.[26] It can be seen from Table 5 that only 49% of drugs were released in the case of ALD/TPA/SBA-15, while in the case of ALD/SBA 15, it shows faster release, which further supports the results obtained from the *in vitro* release study.

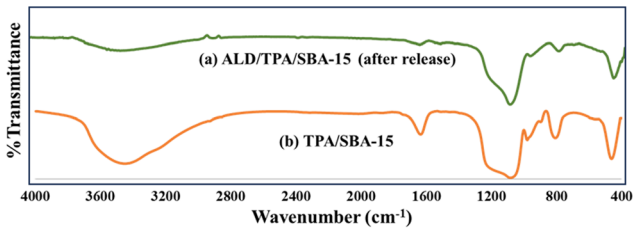

Fig. 10 FT-IR spectra of (a) ALD/TPA/SBA-15 and (b) TPA/SBA-15 after the release study, showing that the structure remains intact even after drug release.

Table 4 Comparison of the release profile of the marketed formulation (Osteofos) with that of ALD/TPA/SBA-15

	% Release (pH 7.4, 37 °C, and stirring conditions)		
Materials	Initial	Up to 3.5 h	Up to 7.5 h
Marketed Formulation (Osteofos)	100%	—	—
ALD/TPA/SBA-15	11%	50%	99%

Table 5 Release studies in dissolution apparatus

Materials	% Release (pH 7.4, 37 °C, and stirring conditions), 0.5 h
ALD/SBA-15	67%
ALD/TPA/SBA-15	49%
Marketed formulation (Osteofos)	100%

 © 2024 The Author(s). Published by the Royal Society of Chemistry

Open Access Article. Published on 01 August 2024. Downloaded on 10/16/2025 6:11:21 PM.
This article is licensed under a Creative Commons Attribution-NonCommercial 3.0 Unported Licence.

The designed system, ALD/TPA/SBA-15, proves to be excellent from all the above studies. Therefore, it is being carried forward to investigate further studies, which include reaction kinetics and cytotoxicity studies.

Release kinetics and mechanism

To study the drug release kinetics and mechanism, the data obtained from the release study of ALD from ALD/TPA/SBA-15 were fitted in different models, as detailed in Table 6.

Here, Q_t is the amount of drug dissolved in time t, Q_0 is the initial amount of drug in the solution (most times, $Q_0 = 0$), and K_0, K_1 and K_H are the release rate constants, respectively.

Zero order release kinetic model

The cumulative drug release is plotted against time to analyze the drug release kinetics. The slope of this plot indicates the zero-order rate constant, while the correlation coefficient constant addresses whether or not drug release follows zero order kinetics. Fig. 11 depicts a zero-order release kinetic model for the ALD/TPA/SBA-15 system with an $R^2 = 0.9976$.

First order release kinetic model

This model depicts the dissolution of drugs contained in porous matrices. The rate of release is concentration-dependent. A log per cent remaining data was plotted against time for ALD/TPA/SBA 15, depicted in Fig. 12. The correlation coefficient of ALD/TPA/SBA-15 was found to be $R^2 = 0.8951$.

Table 6 Mathematical model of drug release

Model	Equation
Zero order	$Q_t = Q_0 + K_0 t$
First order	$\text{Log}\, Q_t = \log Q_0 - K_1 t/2.303$
Higuchi model	$Q_t = K_H \times t_{1/2}$

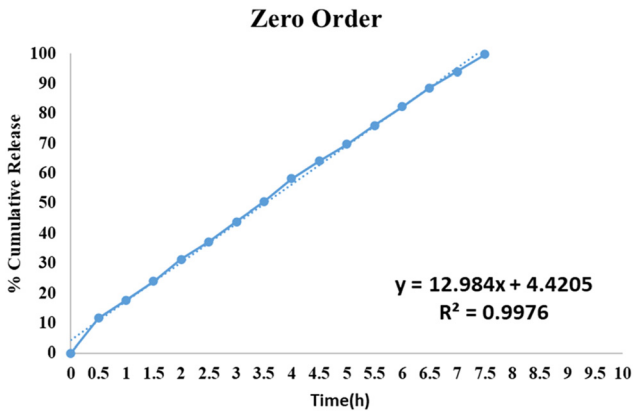

Fig. 11 Zero order release kinetic model of ALD/TPA/SBA-15, which shows the plot of cumulative drug release against time.

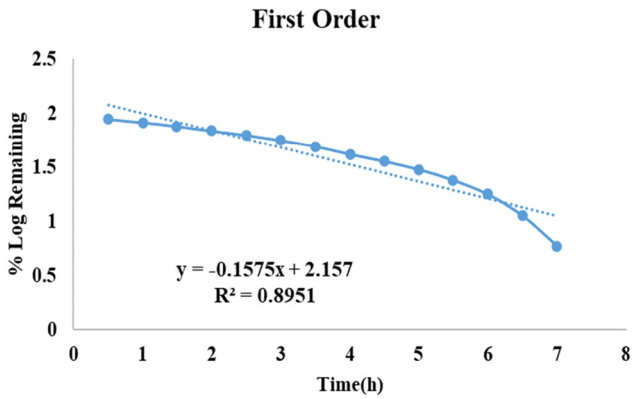

Fig. 12 First-order release kinetic model of ALD/TPA/SBA-15 shows the plot of the log per cent remaining data plotted against time.

Higuchi model

This model deals with the release of drugs from the matrix. According to this model, drug release involves the simultaneous penetration of SBF into the pores, dissolution of drug molecules and diffusion of these molecules from the pores. The correlation coefficient for the Higuchi Model (Fig. 13) for the ALD/TPA/SBA-15 system was $R^2 = 0.9791$. Thus, ALD release from ALD/TPA/SBA-15 follows Fickian diffusion.

Thus, regarding kinetics and mechanism, ALD release from the ALD/TPA/SBA-15 system follows zero-order kinetics and the Higuchi diffusion model.

Evaluation of *in vitro* cytotoxicity – MTT assay

To study the cytotoxic effect of ALD/TPA/SBA-15, an MTT assay was carried out using an MG-63 cell line (Osteosarcoma). At the end of the analysis, a purple-coloured formazan was formed by metabolically active cells, and the intensity of colour demonstrated the functional state of mitochondria. Analysis showed that with increased concentration, the cell viability decreases due to the anti-tumour properties of ALD (Fig. 14). At a dosage of 50 μg mL^{-1}, it shows 16% toxicity,

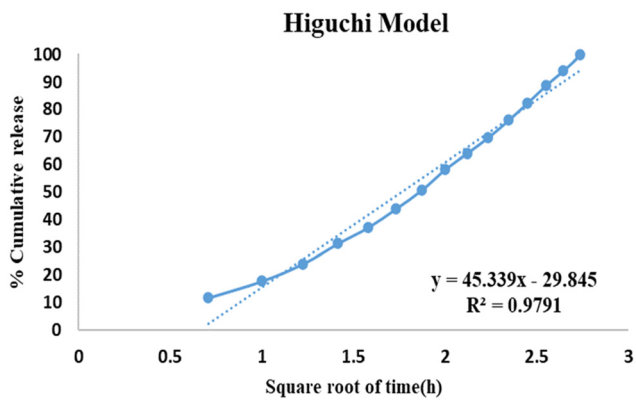

Fig. 13 The Higuchi model of ALD/TPA/SBA-15 shows the plot of cumulative drug release against the square of time.

Open Access Article. Published on 01 August 2024. Downloaded on 10/16/2025 6:11:21 PM.
This article is licensed under a Creative Commons Attribution-NonCommercial 3.0 Unported Licence.

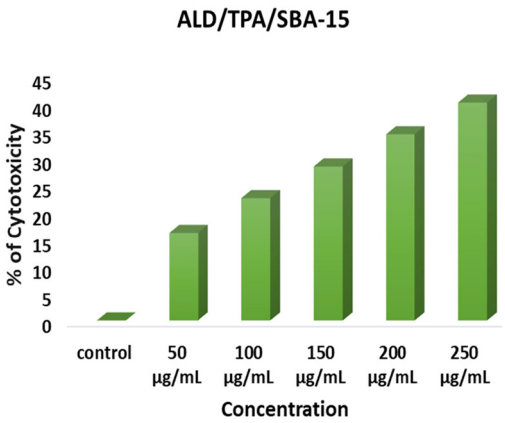

Fig. 14 Cytotoxicity evaluation of ALD/TPA/SBA-15 to observe the cell viability at different concentrations.

while at a dosage of 250 µg mL^{-1}, it shows 40% cytotoxicity. Further, results indicate that osteosarcoma cell proliferation was inhibited significantly at an IC_{50} value of 7.04 µg mL^{-1}. Overall, it can be said that drug-loaded carriers can help reduce tumour growth in bone and osteoclast activity. Images (Fig. 15) show viable cells at different concentrations.

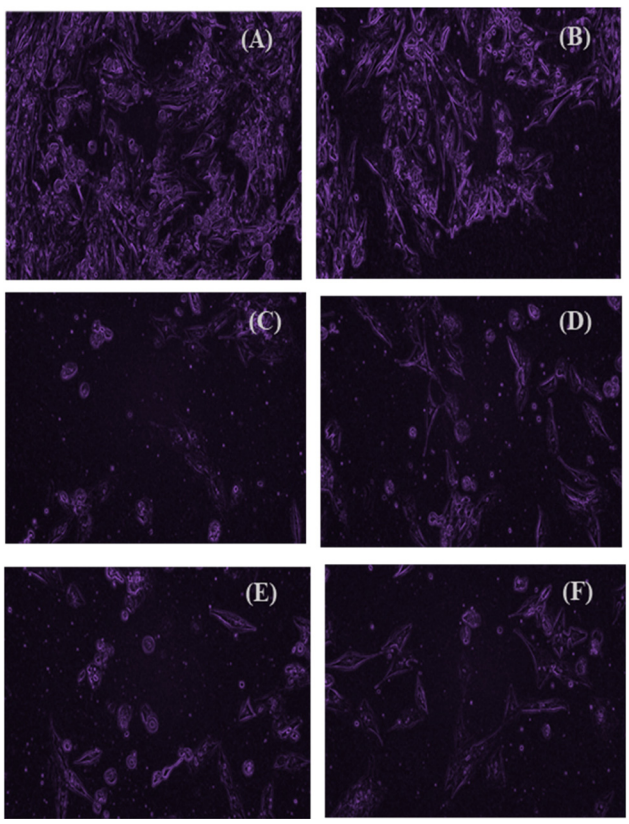

Fig. 15 (A) Control cell, (B) 50 µg mL^{-1} treated cells, (C) 100 µg mL^{-1} treated cells, (D) 150 µg mL^{-1} µg treated cells, (E) 200 µg mL^{-1} treated cells, (F) 250 µg mL^{-1} treated cells. Images showing apoptosis at different concentrations for ALD/TPA/SBA-15.

Novelty of the designed delivery system

The novelty of the present work is that SBA-15 was functionalized with the inorganic moiety TPA for the controlled release of the anti-osteoporotic drug ALD. The release profile of ALD/TPA/SBA-15 was compared with that of the marketed formulation, conveying that the present system is better and exhibits slower drug release. Also, it can be seen from the literature that the increased osteoclast activity is related to the aggressiveness of osteosarcoma. Thus, the designed system can be used for the treatment of osteosarcoma along with osteoporosis as this system shows toxicity towards the osteosarcoma cell line.

Conclusions

The paper describes the synthesis of ALD/TPA/SBA-15, its characterization, and *in vitro* release studies. The release profile shows that controlled drug release was observed for ALD/TPA/SBA-15. The FT-IR spectrum of ALD/TPA/SBA-15 after release shows that TPA acts as a functionalizing agent, and its structure remains intact after drug release. Further, ALD release follows zero-order kinetics, followed by the Higuchi model with Fickian diffusion. Moreover, the results obtained from the MTT assay demonstrate the inhibitory potential of ALD on osteosarcoma. It significantly inhibits tumour cell proliferation, and the results were consistent with other reports, which show that N-BP inhibits tumour cell growth. Therefore, the designed system, ALD/TPA/SBA-15, can be a promising candidate for inducing bone cancer apoptosis and inhibiting bone resorption. Moreover, *in vivo* studies are required to optimize the dosing regimen of the designed system to exploit the anti-tumour property fully.

Author contributions

Anjali Patel: conceptualization, writing – review & editing, supervision, visualization. Shivangi Mehta: methodology, software, writing – original draft, validation, investigation.

Data availability

The data that support the findings of this study are available from the corresponding author upon reasonable request.

Conflicts of interest

The authors declare no conflict of interest.

Acknowledgements

AP and SM are thankful to the Department of Chemistry, the Maharaja Sayajirao University of Baroda for the infrastructural

 © 2024 The Author(s). Published by the Royal Society of Chemistry

Open Access Article. Published on 01 August 2024. Downloaded on 10/16/2025 6:11:21 PM.
This article is licensed under a Creative Commons Attribution-NonCommercial 3.0 Unported Licence.

facilities and for TGA as well as FTIR analysis. SM is thankful to SHODH (ScHeme of Developing High Quality Research) (Ref No: 2022017233). We are also thankful to Avinashilingam Institute for Home Science and Higher Education for Women, Coimbatore for MTT assay.

References

1 C. Christodoulou and C. Cooper, *Postgrad. Med. J.*, 2003, **79**(929), 133–138, DOI: 10.1136/pmj.79.929.133.
2 I. Akkawi and H. Zmerly, *Joints*, 2018, **6**(02), 122–127, DOI: 10.1055/s-0038-1660790.
3 T. Rachner, S. Khosla and L. Hofbauer, *Lancet*, 2011, **377**(9773), 1276–1287, DOI: 10.1016/S0140-6736(10)62349-5.
4 J. Lin and J. Lane, *Clin. Orthop. Relat. Res.*, 2004, **425**, 126–134, DOI: 10.1097/01.blo.0000132404.30139.f2.
5 K. Joanna and L. Joanna, *Int. J. Nanomed.*, 2022, **17**, 6065–6094, DOI: 10.2147/IJN.S388430.
6 B. Aderibigbe, I. Aderibigbe and P. Popoola, *Pharmaceutics*, 2017, **9**(1), 2, DOI: 10.3390/pharmaceutics9010002.
7 A. Doadrio, A. Salinas, J. Sanchez-Montero and M. Vallet-Regi, *Curr. Pharm. Des.*, 2015, **21**(42), 6213–6819.
8 V. Vavsari, G. Ziarani and A. Badiei, *RSC Adv.*, 2015, **5**(111), 91686–91707, DOI: 10.1039/c5ra17780d.
9 F. Balas, M. Manzano, P. Horcajada and M. Vallet-Regí, *J. Am. Chem. Soc.*, 2006, **128**(25), 8116–8117, DOI: 10.1021/ja062286z.
10 M. Colilla, I. Izquierdo-Barba and M. Vallet-Regí, *Microporous Mesoporous Mater.*, 2010, **135**(1–3), 51–59, DOI: 10.1016/j.micromeso.2010.06.010.
11 L. Ochiuz, M. Luca, I. Stoleriu, M. Moscalu, D. Timofte, G. Tantaru and A. Stefanache, *Farmacia*, 2016, **64**(1), 131–134.
12 R. Nechikkattu, S. Park and C. Ha, *Microporous Mesoporous Mater.*, 2019, **279**, 117–127, DOI: 10.1016/j.micromeso.2018.12.022.
13 M. Aureliano, *BioChem*, 2022, **2**, 8–26, DOI: 10.3390/biochem2010002.
14 H. Shah, S. Joshi, A. Haider, U. Kortz, N. Rehman and J. Iqbal, *RSC Adv.*, 2015, **5**(113), 93234–93242, DOI: 10.1039/C5RA18489D.
15 M. Čolović, M. Lacković, J. Lalatović, A. Mougharbel, U. Kortz and D. Krstić, *Curr. Med. Chem.*, 2020, **27**(3), 362–379, DOI: 10.2174/0929867326666190827153532.
16 P. Clézardin, *Bone*, 2011, **48**(1), 71–79, DOI: 10.1016/j.bone.2010.07.016.
17 D. Heymann, B. Ory, F. Gouin, J. Green and F. Rédini, *Trends Mol. Med.*, 2004, **10**(7), 337–343, DOI: 10.1016/j.molmed.2004.05.007.
18 S. Pathan, P. Solanki and A. Patel, *Microporous Mesoporous Mater.*, 2018, **258**, 114–121, DOI: 10.1016/j.micromeso.2017.09.012.
19 D. Dasgupta, M. Das, S. Thakore, A. Patel, S. Kumar and S. SeshadriInt, *J. Drug Delivery Sci. Technol.*, 2022, **72**, 103419, DOI: 10.1016/j.jddst.2022.103419.
20 E. Taha and E. Youssef, *Chem. Pharm. Bull.*, 2003, **51**(12), 1444–1447, DOI: 10.1248/cpb.51.1444.
21 N. Alarfaj, S. Razeq and F. Qahtani, *Asian J. Chem.*, 2011, **23**(2), 697–700.
22 T. da Silva, D. Pereira, B. de Carvalho Patricio, M. Sarcinelli, H. Rocha, S. Letichevsky, C. da Silva and R. Mendonça, *J. Appl. Polym. Sci.*, 2021, **138**(28), 50678, DOI: 10.1002/app.50678.
23 P. Albu, S. Doca, A. Anghel, G. Vlase and T. Vlase, *J. Therm. Anal. Calorim.*, 2017, **127**, 6, DOI: 10.1007/s10973-016-5745-7.
24 V. Brahmkhatri and A. Patel, *Appl. Catal., A*, 2011, **403**(1–2), 161–172, DOI: 10.1016/j.apcata.2011.06.027.
25 Y. Luo, Z. Hou, R. Li and X. Zheng, *Microporous Mesoporous Mater.*, 2008, **109**(1–3), 585–590, DOI: 10.1016/j.micromeso.2007.05.008.
26 R. Uddin, N. Saffoon and K. Sutradhar, *Int. J. Curr. Biomed. Pharm. Res*, 2011, **1**(4), 201–207.

© 2024 The Author(s). Published by the Royal Society of Chemistry